Chapter 7

Multi-Scale Analysis of Angiogenic Dynamics and Therapy

Levon Arakelyan, Yifat Merbl, Peteris Daugulis, Yuval Ginosar, Vladimir Vainstein, Vera Selitser, Yuri Kogan, Hila Harpak, and Zvia Agur
Institute for Medical Biomathematics (IMBM), Bene Ataroth (Israel)

7.1 Introduction

Growth of malignant tumours beyond the diameter of 1 to 2 mm critically depends on their neovascularization, which provides vital nutrients and growth factors,

1-58488-361-8/03/$0.00+$1.50

and also clears toxic waste products of cellular metabolism [1]. Indeed angiogenesis — the formation of new blood vessels by budding from existing ones — has been proven to have a widespread significance in clinical oncology. Its role as a target for cancer therapy, first recognised by Folkman in 1971 [2], has received wide acceptance in the early 1990s following the discovery of the first specific antiangiogenic substances by O'Reilly et al. [3,4]. This therapeutic approach seems advantageous in being universal for different solid tumours and in lacking prominent side effects.

Intensive research during the last 15 years has led to a better understanding of this process and to a recognition of its complexity [5–12]. Major determinants of new vasculature formation are genetic features as well as nutrient availability. Moreover, vascular endothelial growth factor (VEGF) and other stimulatory factors are involved in the regulation of endothelial cell (EC) proliferation and migration [13–20]. The dynamics of the tumour vasculature are not merely the consequence of newly formed vessels, but also of immature vessels transformation into mature ones and the reverse process of destabilisation. Immature vessels may also regress in response to certain stimuli.

In order to establish successful antiangiogenic treatment protocols, the dynamics of angiogenesis must be better understood [21]. But, as was mentioned above and will be further demonstrated, the comprehensive angiogenesis dynamics are too complex to be captured by intuition alone, since they involve several interacting oscillatory processes, which operate on several scales of time and space.

Theory of population dynamics in perturbed environments suggests that oscillatory disease processes can be efficiently controlled when the natural temporal process of the disease is antagonised by an additional, externally imposed, temporal process. The latter can be either a natural process, e.g. the host immune system response in the control of African trypanosomiasis parasitaemia [22], or an artificial one, e.g., a well controlled periodicity of vaccination or chemotherapy efforts, as in the case of measles "pulse vaccination strategies" [23,24], HIV chemotherapy [25,26], or cancer chemotherapy [27–29].

In the present chapter we show how mathematical theory can contribute to the understanding of antiangiogenic therapy. We do so by briefly describing how mathematical models for the angiogenic dynamics are constructed, and subsequently calculated numerically. We begin by elaborating on the complexity of angiogenesis and analysing some empirical results which relate to tumour growth and its vasculature development, thus illustrating this complexity. Then we move to discuss the importance of modelling angiogenesis and present some alternatives for such modelling. These alternatives are tested for their ability to demonstrate and explain phenomena observed empirically. Using these models we test the potential effects of various drugs and drug schedules on the biological system. We then close by introducing some already accomplished applications of such models, along with suggesting further potential applications.

7.2 Defining the Challenge

As mentioned above, intensive research has led to recognition of this complex process [5–12]. Fundamentally, the genetic features of the tumour and the availability of the nutrients are the major determinants of new vasculature formation. Those determinants affect through mediators in the form of growth factors. Under conditions of nutrient deprivation, tumour cells secrete stimulatory factors such as VEGF, a potent stimulator of EC proliferation and migration [13–20]. Consequently, additional blood vessels are formed and the signal for increased VEGF production disappears. VEGF expression will now return to its basic, genetically determined level. The fate of the newly formed blood vessels will depend on this basic VEGF level. If lower than a certain given survival threshold, they will undergo regression [30–32]. This negative feedback can produce successive cycles of growth and regression of blood vessels [33].

Direct *in vivo* experiments show that newly formed blood vessels are dynamic structures, continuously undergoing growth and regression [34,35]. This dynamic instability can come to an end by vessel maturation, a process where immature vessels are covered by pericytes [34,35], which is governed by platelet derived growth factor (PDGF) and the angiopoietin system [36–40]. The significance of the angiopoietin system in vessel maturation has recently become clear [38–40]. This system includes Tie-2, the endothelium-specific receptor tyrosine kinase, its agonist, angiopoietin-1 (Ang1), and its natural antagonist angiopoietin-2 (Ang2). Ang1 promotes vessel maturation, while Ang2 antagonises its action and can destabilise mature vessels [36,37]. Ang1 and Ang2 can be expressed variably in EC or in human tumour cells, depending on the individual tumour type [36,37,41,42]. Hence, the expression of VEGF, Ang1, Ang2, as well as PDGF, can be influenced by both genetic and micro-environmental factors.

From the description above, it is clear that the angiogenesis process involves several interactive sub-processes, namely tumour growth and regression, nutrient-dependent production of angiogenic factors, vascular growth and regression, vessel maturation, and destabilisation of mature vessels. Several angiogenic factors should be taken into account, including VEGF, PDGF, Ang1, Ang2, and possibly more. Moreover, the system is comprised of three scales (levels) to be considered; the molecular level, the cellular level, and the tissue level. Hence, its modelling is a multi-scale modelling. To demonstrate the complexity of the issue, we bring some experimental data, of which analysis was performed. The analysis shows the need for modelling tools in order to fully understand empirical results, all the more so if one wishes to predict or even manipulate treatment results.

7.2.1 Analysis of Experimental Results

In order to better understand the dynamics of vascular development and tumour growth, analysis was conducted on experimental results, using mathematical and statistical tools.

7.2.1.1 Description of the experiment

The data given were of an experiment performed in M. Neeman's laboratory at the Weizmann Institute, Israel [33,43]. The experiment was conducted on 11 mice, and included subcutaneous implantation of a tumour spheroid in a specific location in the mouse's body and following its growth and angiogenesis, including vessel maturation and functionality [44].

In essence, the data supplied contained:

1. Tumour volume
2. Vessel density – total
3. An estimate of the fraction of functional (perfused) vessels
4. An estimate of the degree of maturation of the vessels

Magnetic resonance imaging (MRI) was used for measuring tumour growth and blood vessel density. The functionality of vessels was assessed by MRI signal intensity changes in response to an elevated oxygen level, while the maturation of vessels was assessed by MRI signal intensity changes in response to an elevated carbon dioxide level. These tests were performed in several measurement points inside the tumour and in certain locations in the body, relative to the tumour. These measurement points (see Figure 7.1 for the definition of reference points in the mouse's body (left) and in the tumour (right)), are specified herein by order from inside the tumour to the furthest point checked:
In – Inside the tumour spheroid
Rim – Any point located within the 1 mm wide rim around the tumour spheroid
Cn – A close reference site, within 7 mm distance from the tumour spheroid
Cf – A further distant reference site yet in the same tissue

7.2.1.2 Data processing

The above data were processed and prepared for analysis, in the following way:

- Tumour volume was measured in mm^3.
- Total vessel density was presented as the average vessel density (AVD). Signal intensities (S) were measured within the 1 mm diameter vicinity (Rim) of the implanted tumour as well as in a control region about 7 mm away from

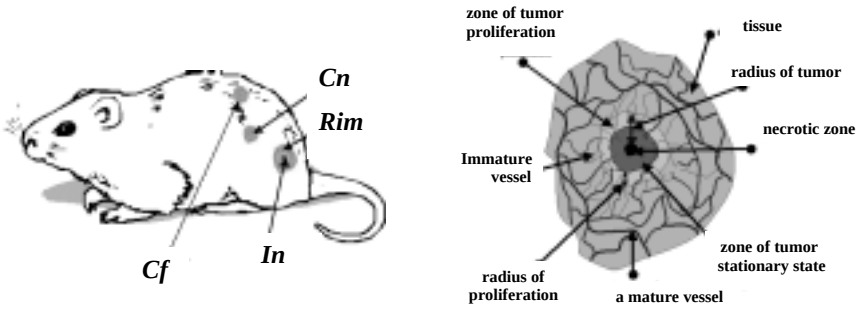

Figure 7.1

Left- The nomenclature of locations in the mouse's body. Right- schematisation of the tumour and its close vicinity, demonstrating the radius measured for tumour volume calculations and mature and immature vessels in its immediate vicinity.

the tumour (Cn), serving as a reference point. AVD was calculated as $1 - ln(S_{Rim}/S_{Cn})$. The outcome of this processing reflects in percentage the degree by which AVD is higher or lower than the normal level measured in the healthy tissue (at Cn).

- F (functionality) reflects the density of perfused (mature + immature) vessels in a certain tested area. The calculation of parameter F is performed using MRI measurements. As mentioned above, these measurements were performed separately for each of the four location points defined. Under the "calculating parameter values" section will be further demonstration of the application of readings in different locations within the same mouse.

- Similarly, M (maturation) reflects the maturation level of the vessels in the area tested. The calculation of parameter M is performed using MRI measurements. Also in common with F, maturation measurements were performed separately for each of the four location points defined above. The use of which will be explained below.

7.2.1.3 Calculating parameter values

We defined several parameters, for later use, characterising the tumour and representing interrelations between the selected aspects of its growth and vascularity. For example, the rate of tumour growth was defined as:

$$\text{Tumour growth rate } = \left(\frac{Vtum(X)}{Vtum(X-1)}\right)^{\frac{1}{Time(X)-Time(X-1)}},$$

where X represents the measurement day.

In addition, the reference points Cn and Cf were checked in order to serve as control over changes in readings that are immaterial to the progress of the disease. In order to apply this, several parameters were calculated. This was carried out firstly by calibrating the readings in points Rim or In, using the same day and mouse readings of one of the two reference points. Two parameter examples are:

1. $M_{\frac{Rim}{Cn}}$ – denotes the calibration of a result reflecting density of mature vessels in Rim using the reading in Cn as a reference point.
2. $F_{\frac{In}{Cf}}$ – denotes the calibration of a result reflecting density of functional (perfused) vessels in *In* using the matching reading in Cf as a reference point.

Secondly, a calibration was performed over maturation test results in comparison with functionality results. This is in order to render the numerical results equivalent. The source of this necessity was that maturation and functionality values are retrieved using different procedures and may elicit numerically incomparable results, though in normal tissue they reflect identical amounts of vessels. This was solved by calculating the ratio between matching readings of both maturation and function, performed in the normal tissue (either Cn or Cf) since these two values are expected to be practically equal. After such a ratio was defined (marked as K), it served as a correction factor for these above mentioned values, for example: $K = M_{Cf}/F_{Cf}$.

7.2.1.4 Data analysis

While observing *in vivo* tumour sizes depending on time (Figure 7.2), three growth behaviours are apparent, differing in growth rate. Thus, mice were assigned to three groups, according to differences in growth rates and growth patterns:

- Fast growing group: The mice in this group show continuous, rapid tumour growth with no fluctuations observed in tumour size. These mice died first, around 20 days from implantation.
- Medium growing group: The mice in this group started a relatively slow tumour growth, which increased past some point. The growth was characterised by occasional mild fluctuations. Their survival was intermediate, in most cases (19 to 36 days).
- Slow growing group: These mice showed a slow tumour growth rate. In addition, many fluctuations in size were apparent during their growth. These mice survived the longest, over 70 days.

7.2.1.5 Interconnecting tumour growth rate with AVD

Further analysis was performed, by observing the relations between tumour growth rates and AVD. This was done separately for each of the three growth pattern groups. Figure 7.3 relates to the fast, medium, and slow groups in the upper, middle,

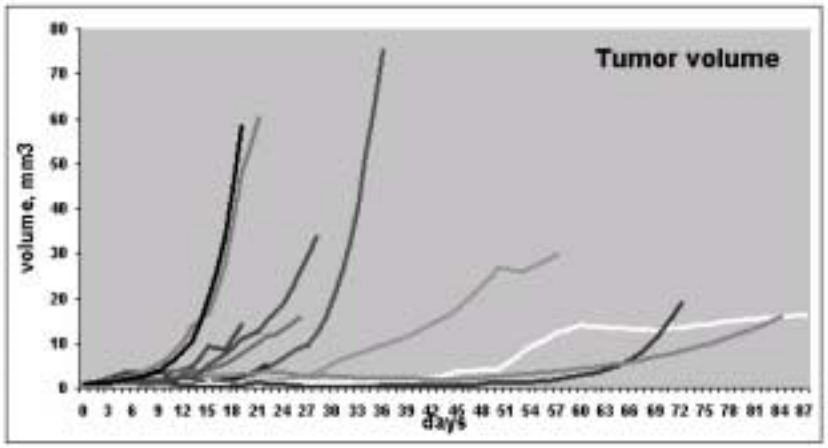

Figure 7.2

Course of *in vivo* tumour growth. Tumour volume designated in mm^3 depending on time in days. Each curve describes growth of one tumour, implanted in one mouse.

and lower parts, respectively. In the left part of Figure 7.3 are the layouts of tumour growth rate and AVD results, per each reading performed, per each of the mice in the group. There is no indication of the time point in the experiment at which these readings were performed. This is because we are here interested in researching the relation between AVD and tumour growth rate, independent of time. In each of the groups, three to four mice are presented, each marked by a different shape. After the layout was complete, the boundaries within which these points distributed were marked by dashed lines. Per each of the three groups, an additional graph is presented on the right side of Figure 7.3, showing the course of growth, i.e., tumour volume depending on time, of one mouse of that group. Note that the scales of these three graphs (upper, middle, and lower Figure 7.3, on the right) are different, a result of the vast differences in the growth rates.

The values of all readings of all three mice of the first group (the upper graphs) had a minimal tumour growth rate value of one, as appears from the marked inclusive range. Hence, there was no measurement where the tumour was found to have regressed in size, rather it grew constantly from one measurement to the next.

In the example of a specific mouse of this group (upper-right) it is seen that the volume increased rapidly and indeed, continuously, reaching a maximum of 60 mm^3 in about 20 days.

As for the reading range of AVD values, it was between 0.665 to 1.2. This relatively dense appearance (in comparison with the other groups) corresponds to a constant growth without the fluctuations observed in other groups.

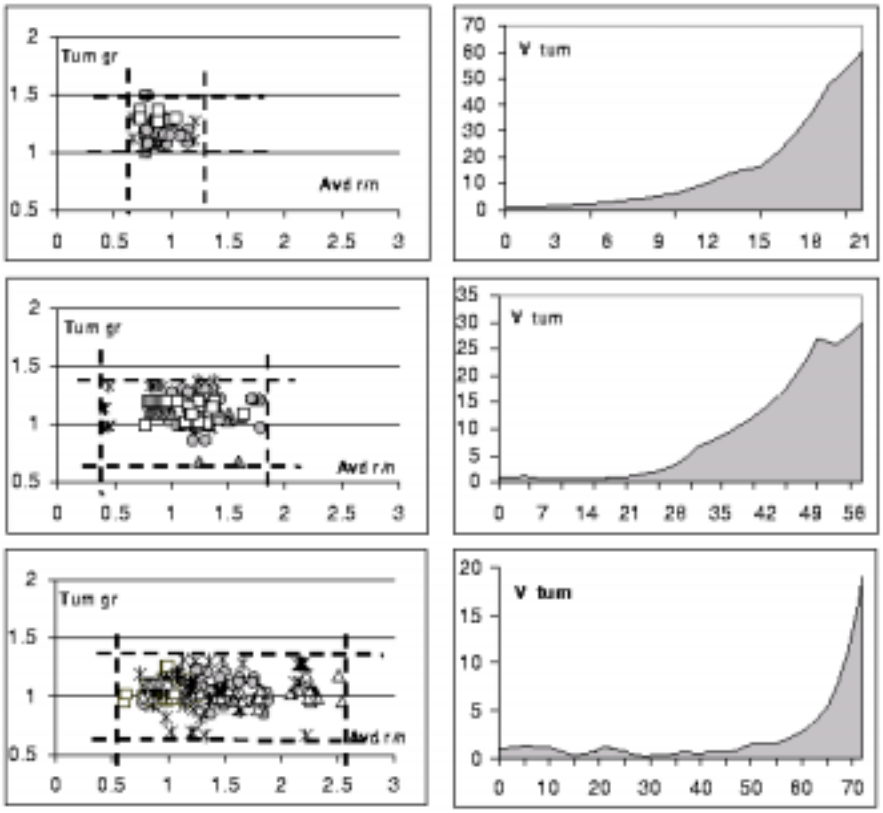

Figure 7.3

The left column, upper, middle, and lower, contains coordinates of all readings performed in the fast, medium, and slow growing groups, respectively. The points depict the values of growth rate coinciding with AVD. In these figures, the results of each individual mouse are marked by a different shape. The boundaries within which all points of a group are distributed, are marked by dashed lines. The right column, upper, middle and lower graphs, show the tumour volume (mm^3) depending on time (days), i.e., the course of growth, of a single individual mouse in the corresponding group. Note that the scales of these three graphs are different, a result of the vast differences in the growth rates.

Both the second and the third groups had a wider range of tumour growth rates, with some of their values lower than one, indicating a decrease in tumour volume. The AVD ranges were also wider in these two groups, with the third group having the widest range of both growth rate and AVD, as well as the most intense fluctuations in the tumour development. Note that in these two groups, one may find, on both ends of the AVD range, readings of growth rate either over or under unity. This indicates that there is no clear association between AVD value and the tumour growth trend (rate over one, indicating increase or rate under one, indicating decrease). Below we introduce the concept of using a time delay assumption in the analysis of these data. This might enable establishing a relation between the two factors: tumour growth and vessel density.

When observing the individual examples of mice from the second and third groups, a slower growth rate compared with that of the first group is apparent. While in the mouse of the first group a maximum of 60 mm^3 was reached in 21 days, in the mouse of the second group the tumour size was about 1 mm^3 after 20 days and reached a maximum of about 30 mm^3 within 55 days. As for the individual mouse of the third group, tumour size was kept at a minimum around 1 mm^3 for about 50 days, and grew to only 20 mm^3 after 70 days. While some fluctuations are observed in the individual reading of the second group (some regression around the day five), much more prominent fluctuations are demonstrated in the mouse from the third group.

From these observations, it seems that fluctuating and slow growth typically is associated with drastic changes of AVD, within a relatively wide range. Clearly, AVD is a crucial factor influencing tumour growth, and there is a mutual effect between the two processes. Hence, it biologically makes sense that when a phenomenon of fluctuation in size is observed, drastic changes are also apparent in AVD measurements, playing both roles of effector and consequence. It would be interesting to find a correlation between any of the relevant values measured here.

7.2.1.6 Correlation tests

The correlations between tumour growth rate and variants of vessel density were calculated (Microsoft Excel, see Table 7.1), as well as between tumour size and the same variants of vessels density (data not shown). As demonstrated in the previous section regarding calculating parameter values, density relates to either mature vessels or to functional vessels (i.e., those that were estimated *in vivo* to be perfused by blood). These density readings, performed in a choice of locations in the tumour, are then calibrated using different options for reference points (see Figure 7.1). Hence, there is a variety of measurement results for "vessel density" depending on the type of vessels tested, the location of the testing point in the tumour, and the choice of its reference point. A result of 0.4 to 0.6 indicated an intermediate correlation while a result of 0.6 and higher represented a strong correlation. As apparent in Table 7.1, no correlation was found without time delay, while after introducing time delay into the calculations, either an intermediate correlation ($M_{I/f}, M_{o/f}$) or a strong one ($F_{I/f}, F_{o/f}$), was found (see below for elaboration on the concept of time delay). One may notice that in the case of mature vessels ($M_{I/f}, M_{o/f}$) the correlation was

Table 7.1 The correlation between the tumour growth rates (Ktg) and vessel density parameters ($M_{i/f}, M_{o/f}, F_{i/f}, F_{o/f}$) of all readings of a specific mouse, "P." $M_{I/f}$: Mature vessel density in point In vs. point Cf. $M_{o/f}$: Mature vessel density in point Rim vs. point Cf. $F_{I/f}$: Functioning vessel density in point In vs. point Cf. $F_{o/f}$: Functioning vessel density in point Rim vs. point Cf. These correlations were calculated both with and without time delay. The time delay of 3 days was found to be optimal for some of the parameters while time delay of 4 days was found optimal for the others.

Mouse "P"				
	K tg ~ M i/f	K tg ~ M o/f	K tg ~F i/f	K tg ~ F o/f
without time delay	-0.174706611	0.059830672	0.305976706	0.095252136
time delay of 3-4 days	-0.493741611	-0.460786427	0.644311185	0.670577493

negative, reflecting destabilisation of the vessels in response to tumour growth.

7.2.1.7 The concept of time delay

Both the correlation table (7.1) and the previous observation that large changes in AVD seem to correlate with slow and typically fluctuating growth (Figure 7.3), appear to point to a physiologically expected relation between growth behaviour and vasculature. Nevertheless, it is clear that a change in AVD cannot immediately affect the tumour size and neither will changes in tumour size immediately affect the vessel number. Rather, there must be a genetically and environmentally determined kinetics dictating the characteristic time by which tumour growth will respond to changes in AVD, and vice versa. Hence, the next step in our analysis was to investigate the role of different putative time-delays between changes in vessel density and tumour growth rate. This will serve the purpose of disentangling the above described intricate dynamics, and will enable the unification of the different angiogenesis sub-processes into one picture. This means that instead of observing the relations between AVD and tumour growth rate of the same reading, on the same day, the growth rate was checked to correlate with the vessel density reading of some specific time earlier or later. At this phase, the search concentrated on finding the time delay at which results were to be observed, so that the relation between vessel density and growth rate was best established.

The method used for testing the effect of time delays was a mathematical calculation using a correlation function (again, Microsoft Excel). Since the experiment performed consisted of implanting an avascular tumour, which further developed vasculature, we chose to test the dependence of vessel densities (whether functional or mature) upon tumour growth. Hence, per each mouse, different time delay options were checked by testing the correlation function (data not shown), between AVD/F/M readings of certain days and the tumour growth on the suggested preceding day. We then searched for the best time delay for each mouse, which were not identical among all mice (data not shown).

7.2.1.8 Testing the effects of time delay on the analysis outcomes

Vascular densities of different categories of vessels, mature or functional, were calibrated for each individual mouse, according to the described in "calculating parameter values" above, similarly to the process preceding the correlation tests. For example, $M_{I/f}$, stands for density of mature vessels in area In calibrated according to readings in area Cf. In addition to vascular density readings, tumour volume was measured as well ($Vtum$). To demonstrate the relation between vascular density measurements and $Vtum$, we bring the diagrams in Figure 7.4, relating to the previously mentioned mouse. Measurements for each of the different vascular density categories are represented by a curve. Entries whose coordinates are vascular density (y axis) and $Vtum$ (x axis) of each measurement, were connected according to the chronological order in which the measurements were taken, yielding a curve which unfolds with time. This type of representation is denoted "phase plane." In upper Figure 7.4, the diagram was constructed without any time delay. This means that the entries represent measurements of the same day for both vascular density and $Vtum$. In lower Figure 7.4, on the other hand, the optimal time delay found for this specific mouse (as mentioned in the previous section) was applied into the diagram. Hence, each entry represents a vascular density reading of a given day and a $Vtum$ reading of a day preceding it, by the constant time delay chosen. Please note that the axes are now principally switched compared with Figure 7.3, i.e., here the x axis relates to $Vtum$, and the y axis is AVD.

7.2.1.9 Conclusions from the analysis of the experiments

In both upper and lower parts of Figure 7.4, once $Vtum$ is over a certain size, there appears to be a state of constant growth and no change in any of the vascular density measurements. This is indicated by the lines being rather straight, horizontal, and overlapping in that range of $Vtum$. Nevertheless, as it appears in Figure 7.4 (upper), there is an area of intensive occurrences in the lower range of $Vtum$ i.e., per certain tumour sizes within that range, many different values of vessel densities (y axis) were observed. All the more so, the directions of the lines with time indicate that per the same value of vascular density measurement, one may find the tumour to be either shrinking or in the process of growing. This shows that under the same vascular density conditions, it is not yet determined whether the growth trend shall be negative or positive.

In Figure 7.4 (lower), time delay was introduced into the system; specifically in this case, it was 3 days (optimal time delay found according to the techniques described above). Once applying the time delay into the results, one can appreciate the change in the appearance of the graph, in that the areas of intensive occurrences have cleared up. Instead, oscillations emerge (depicted as a limit cycle behaviour in these phase planes), indicating an interdependent growth behaviour of the two processes.

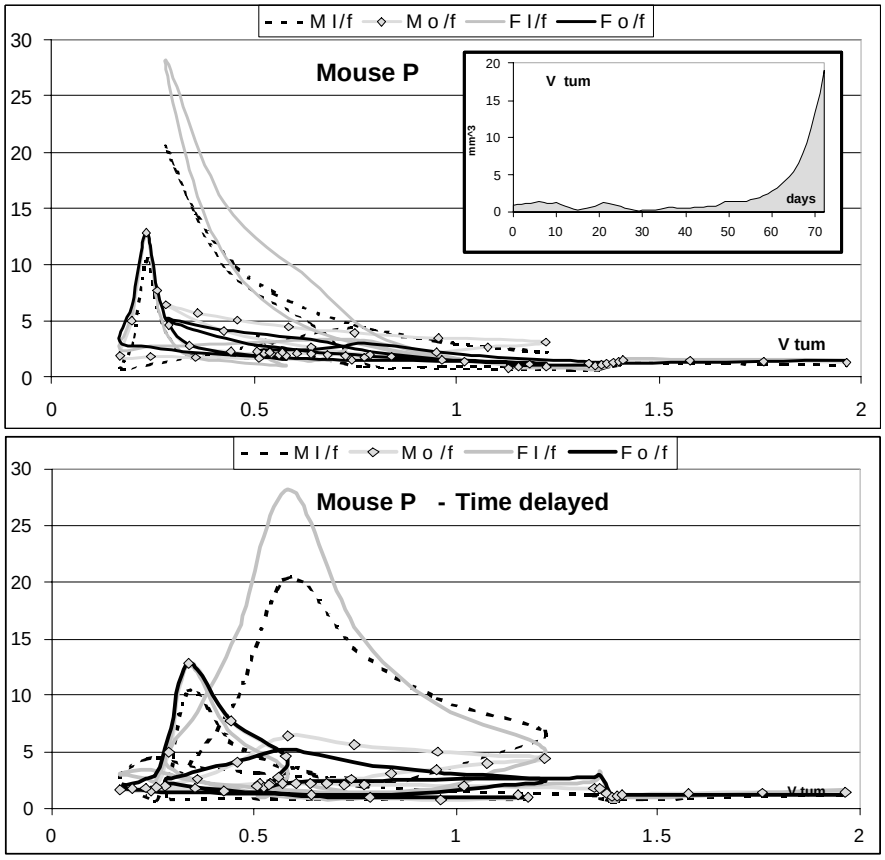

Figure 7.4

Analysis of experimental results of mouse "P," relating vessel density to tumour growth. Vessel density of four different calculated parameters presented as a function of tumour volume ($Vtum$) measurements. $M_{I/f}$: Mature vessel density in point In vs. point Cf. $M_{o/f}$: Mature vessel density in point Rim vs. point Cf. $F_{I/f}$: Functioning vessel density in point In vs. point Cf. $F_{o/f}$: Functioning vessel density in point Rim vs. point Cf. The entries are connected according to their chronological order. Upper: The entries are density and $Vtum$ measured at the same day. Lower: A time delay of 3 days was applied, hence, the entries are created by the measurement of density at a given day and $Vtum$ measured 3 days earlier.

Analysing tumour growth, contrasting growth trends are observed under the same vessel density, as reflected by the lines in Figure 7.4 (lower part, dotted line). In the major loop of $Vtum$ corresponding with $M_{I/f}$ (density of mature vessels inside the tumour, calibrated by their density in reference point Cf) there are two entries where $M_{I/f}$ equals about 7.5. However, in the first entry ($Vtum\ 0.4$) the tumour is in the process of increasing, while the second entry ($Vtum\ 1.2$) is a bifurcation point, where a switch occurs from a phase of growth to a phase of regression in size. This means that a single vessel density entry cannot reflect the trend of tumour growth, which is not monotonic. It is to be expected that more complete analysis of the system can be obtained by separating the involved elements (such as mature vs. immature vessels, or functional vessels etc.) and checking the role of each one of them in dictating the growth status, possibly through regression analysis.

Both maturation and functionality of vessels were separately analysed here, and found to each have the oscillatory behaviour described above. This actually means, that, through the process of tumour growth, both mature vessels category and the functioning vessels category, may transiently undergo regression. The regression of functional vessels is a decrease in the total amount of mature vessels (which are clearly functioning) and of functioning immature vessels. The regression of mature vessels is in essence the process of destabilisation. Hence, our results infer to the fact that immature vessels may undergo regression and mature vessels may undergo destabilisation into immaturity (possibly later leading to regression), even in the course of tumour growth.

Our analysis results (data not shown) suggest that there might be a different time delay between mature and immature blood vessels in correlation with the tumour growth, and this will be further investigated.

7.3 Mathematical Models of Tumour Growth and Angiogenesis

Vascular tumour growth, including dynamics of both vasculature and malignant cells, have been described in mathematical models by Hahnfeldt et al. [45], who propose a macroscopic model, assuming logistic tumour growth. However, this model neither takes into account vessel maturation nor does it allow for the nutrient-dependency secretion of proangiogenic factors. Bellomo and Preziosi [46] and De Angelis and Preziosi [47] describe the vascular tumour system on three scales: molecules, cells, and macroscopic entities (such as tumour volume). The latter model is much more detailed than the previous one [45], however it also does not include maturation of new blood vessels.

In this section, we present two classes of angiogenesis models: continuous models and a discrete model. The continuous models have been fully analysed in [48]. These models generally define three major processes: tumour growth, growth factor

production, and vessel growth. Each model defines the interrelations between the three, with several complexity levels being analysed. The analysis of the different continuous models relates to the empirical findings presented in the previous part. Hence, we are attempting to identify within each of the models the observed phenomenon of tumour size fluctuations accompanied by slow growth. In addition, the importance of including a time delay into the system is being demonstrated.

The *a priori* advantage of the continuous models is their analytic tractability, that is, their solution holds universally, no matter what the precise parameter values are. However, once these models become too complex, we find ourselves lacking the tools for solving them. This trade-off is a constraint, which makes us choose the suitable balance between complexity and applicability. Nevertheless, since our ultimate aim is to provide methods for improving drug treatment of vascular tumours, we must take into account events both on the molecular and the organic levels, without compromising our ability to analyse the global dynamics. This delicate balance is achieved here by using both the analytically tractable models and the more complex discrete models. The former are used for deciphering the universal behaviour of angiogenesis, while the latter are used for making realistic, practical, and empirically testable predictions.

Below we present and analyse several continuous models, which differ in complexity. Subsequently, we present the discrete model, which is complex enough to mimic real life, yet simple enough to enable simulation under many parameter sets. This model implements an algorithm of vascular tumour growth. The algorithm further addresses the complexity described and demonstrated above. This is performed by taking into account all the aforementioned sub-processes constituting the modelled process, along with the effects of several critical growth factors. Modelling is carried out on three scales; the molecular level, the cellular level and the tissue level. As we shall see in the next section, the algorithm used here enables the induction of drug therapy as well.

7.3.1 Continuous Models

In this part we consider angiogenesis models presented by order of increased complexity, which originates from adding dimensions to the system. In addition, time delay is also introduced into the system. Time delay was introduced into the analysis of empirical results in the previous section, and was shown to have a major impact. Similarly, mathematical analysis of these models shows here that in a sense this time delay is mandatory if one wishes to demonstrate the fluctuations observed in experimental results.

7.3.1.1 General assumptions of the models

Each of the models described herein involves the following time dependent variables:

- the number of tumour cells or tumour size (denoted by N)
- the amounts of growth factors known to be involved in angiogenesis supplying the tumour defined as P. For more accurate description, P may be broken down into several growth factors (proteins) which may differ in their effects and/or kinetics
- the effective volume of blood vessels supplying the tumour, which again may either be defined separately for immature and mature vessels or as the total of both, denoted by V

All modelling alternatives are systems of ordinary differential equations with or without time delay. In all of these models we use "sigmoid like" functions — smooth monotonous functions having a horizontal asymptote, e.g., $1/[1 + e^{k(x+s)}]$. These functions describe a response of the system to the relevant biological stimuli affecting it. The reasons for such a choice of the response function are the experimental observations which show that below and above certain thresholds, changes in the intensity of the stimuli have minor effects on the response. Between the threshold values (in the sensitivity region), the process rate depends monotonously on the stimuli value. In our analysis we use only the basic properties of sigmoidal functions, and we do not expect their exact shape to be easily determined from experiments or otherwise.

We assume that the tumour size dynamics is determined by availability of oxygen and nutrients. The amount of nutrients delivered and the oxygen supplied to the tumour is proportional to the volume of blood vessels supplying the tumour, whether inside the tumour or in its close vicinity. To take this into account we use effective vessel density (EVD) which may relate to immature vessels, mature vessels, or the total of both, denoted by E_1, E_2, or E, respectively. EVD is calculated by dividing the corresponding vessel volume by the tumour size $E = \frac{V}{N}$. To simplify our models we assume that vessel wall permeability (perfusion) is the same for immature and mature vessels. For the tumour size dynamics in all our models we assume the Malthusian law determined by

$$\dot{N} = f_1(E)N(t), \tag{7.1}$$

where f_1 is an increasing sigmoid function capturing the processes of cell proliferation and death:

$$f_1(E = 0) < 0, \qquad \lim_{E\to\infty} f_1(E) > 0. \tag{7.2}$$

For dynamics of protein (growth factor) compartments we assume that proteins are produced by tumour cells or immature vessels, and degraded by an intrinsic clearance process. Elaboration of the clearance process will be discussed later, suggesting the introduction of additional consuming elements, such as the forming vessels, into the model.

For dynamics of vessel compartments we assume that it is a superposition of four processes, some are contrasting some of the others: formation of immature vessels, regression of immature vessels, maturation of immature vessels, and destabilisation of mature vessels into immature vessels. We assume that these four processes are driven by sigmoid like responses, as described above, depending on specified proteins. These proteins are the stimuli mentioned earlier as the effectors of these functions.

7.3.1.2 A three-dimensional model with no time delay

The simplest modelling option presented merely captures the three independent variables mentioned earlier: tumour size N, total vessel volume V, and the amount of protein P. The only thing that we assume about the protein is that it drives the vessel formation or regression in a sigmoidal way. The rate of change of N is determined by a Malthusian law sigmoidally depending on E (representing EVD, as defined earlier). The protein P is produced by the tumour at a rate sigmoidally dependent on E and is decaying, by some clearance process as mentioned above, at a constant positive rate δ. The rate of change of the vessel volume V is sigmoidally driven by the protein. Thus we have the system

$$\begin{cases} \dot{N} = f_1(E)N, \\ \dot{P} = f_2(E)N - \delta P, \\ \dot{V} = f_3(P)V, \end{cases} \tag{7.3}$$

where

- f_1 is the tumour cells proliferation rate, it is an increasing function of E and satisfies Equation (7.2).
- f_2 is the protein production rate, it is a decreasing function of E and satisfies

$$f_2(E) > 0\,, \qquad \lim_{E\to\infty} f_2(E) = 0. \tag{7.4}$$

- f_3 is the vessel growth rate, it is an increasing function of P and satisfies

$$f_3(P=0) < 0\,, \qquad \lim_{P\to\infty} f_3(P) > 0. \tag{7.5}$$

To simplify the analysis we make a substitution of variables $V \to E$ and get a system

$$\begin{cases} \dot{N} = f_1(E)N, \\ \dot{P} = f_2(E)N - \delta P, \\ \dot{E} = f_3(P)E - f_1(E)E. \end{cases} \tag{7.6}$$

The next step towards the purpose of mathematically demonstrating the phenomena observed empirically, is the analysis of Hopf bifurcation points. For mathematical background on Hopf points we refer the reader to [49]. To this end, we shall

only clarify, that Hopf points are specific cases of fixed points essentially admitting small oscillations in their vicinity. Their biological equivalent are steady states in which the biological system is expected to demonstrate oscillatory behaviour. Since such a behaviour was observed in the empirical results, it was of high interest to research the existence of such points in each of the systems suggested.

For each set of parameters which determine f_1, f_2, and f_3, the model has one fixed point $Q^{(1)} = (N^{(1)}, P^{(1)}, E^{(1)})$ with $N^{(1)} > 0$, given by

$$f_1(E^{(1)}) = 0\,, \qquad f_3(P^{(1)}) = 0\,, \qquad N^{(1)} = \frac{\delta P^{(1)}}{f_2(E^{(1)})}\,.$$

We claim that there are no Hopf bifurcation points among this family of steady states.

Here is an explanation: the matrix of the system linearised at such a point is

$$M = \begin{pmatrix} 0 & 0 & f_1'(E^{(1)})N^{(1)} \\ f_2(E^{(1)}) & -\delta & f_2'(E^{(1)})N^{(1)} \\ 0 & f_3'(P^{(1)})E^{(1)} & -f_1'(E^{(1)})E^{(1)} \end{pmatrix} = \begin{pmatrix} 0 & 0 & a'N^{(1)} \\ b & -\delta & -b'N^{(1)} \\ 0 & c'E^{(1)} & -a'E^{(1)} \end{pmatrix}, \tag{7.7}$$

where all the new parameters $a' = f_1'(E^{(1)})$, $b = f_2(E^{(1)})$, $b' = -f_2'(E^{(1)})$, and $c' = f_3'(P^{(1)})$ are positive.

We calculate the characteristic equation

$$\det(M - \lambda I) = -\lambda^3 - \lambda^2(a'E^{(1)} + \delta) - \lambda(a'\delta E^{(1)} + b'c'N^{(1)}E^{(1)}) + a'bc'N^{(1)}E^{(1)} \tag{7.8}$$

Hopf points arise when the characteristic polynomial at the fixed point admits a pair of pure imaginary roots. If a cubic polynomial admits such a pair $\pm Ai, A \in \mathbf{R}$ then it has the form

$$-(\lambda^2 + A^2)(\lambda + B) = -(\lambda^3 + B\lambda^2 + A^2\lambda + A^2B), \tag{7.9}$$

for some $B \in \mathbf{R}$. Since the coefficients of $\det(M - \lambda I)$ satisfy $-(a'bc'N^{(1)}E^{(1)}) < 0$ and $a'E^{(1)} + \delta > 0, a'\delta E^{(1)} + b'c'N^{(1)}E^{(1)} > 0$, we have that the characteristic polynomial cannot have pure imaginary roots and thus there are no Hopf points with $N \neq 0$ in Equation (7.6).

7.3.1.3 Introducing time delays into the three-dimensional model

While analysing empirical results (see the above section "analysis of experimental results"), the introduction of time delay elicited the appearance of oscillatory behaviour, as well as improved by far the correlation between two major processes, namely the dynamics of vessel density and tumour growth. This correlation may indicate that the correct way for describing the mutual dependence between the processes must involve time delay. The oscillatory behaviour might also indicate that Hopf points would be found if time delay is introduced into the analytical system. Thus, the next step was to apply time delay and analyse its effect.

Two time delays were introduced: τ_1 in the proliferation/death response to stimuli and τ_2, in the vessel formation/regression response to stimuli.

Let $E_{\tau_1} = E(t-\tau_1), P_{\tau_2} = P(t-\tau_2)$, then system (7.3) is modified, yielding:

$$\begin{cases} \dot{N} = f_1(E_{\tau_1})N, \\ \dot{P} = f_2(E)N - \delta P, \\ \dot{E} = f_3(P_{\tau_2})E - f_1(E_{\tau_1}))E. \end{cases} \tag{7.10}$$

This system has the same fixed points as (7.6). Again we are only interested in the family of fixed points $Q^{(1)}$. The analysis of the behaviour of 7.10 near $Q^{(1)}$ gives rise to the following transcendental analogue of Equation (7.8):

$$\lambda^3 + c_1\lambda^2 e^{-\lambda\tau_1} + \delta\lambda^2 + (c_1\delta)\lambda e^{-\lambda\tau_1} + c_2\lambda e^{-\lambda\tau_2} - c_3 e^{-\lambda(\tau_1+\tau_2)} = 0, \tag{7.11}$$

where $c_1 = a'E^{(1)}, c_2 = b'c'E^{(1)}N^{(1)}, c_3 = a'bc'N^{(1)}E^{(1)}$ are independent positive parameters.

The rigidity of the algebraic equation (7.8) is relaxed in Equation (7.11) by the time delays which appear in the exponential factors. This enables us to find appropriate positive parameters for f_1, f_2, and f_3 such that there are pure imaginary solutions to Equation (7.11). (The computation is not given here and appears in [48].) As already mentioned, existence of Hopf bifurcation points is conditioned by pure imaginary solutions, therefore we deduce that for every $(\tau_1, \tau_2) \neq (0,0)$ the family $Q^{(1)}$ contains Hopf points.

7.3.1.4 A five-dimensional model with time delays

To make our models more elaborate and realistic, we introduce more compartments representing vessels and proteins. First, the inclusive representation of vessels effective volume V, is replaced by separate descriptions of the effective immature and mature vessel volumes denoted by V_1 and V_2, respectively. The values of either vessel subpopulation will be separately analysed. Hence, the model allows both maturation of immature vessels and destabilisation of mature vessels. Secondly, the general term protein, denoted P, is now replaced by two specific proteins namely $VEGF$, denoted P_1 and $Ang1$, denoted P_2. We assume that $VEGF$ is produced by the tumour at a rate sigmoidally dependent on the effective vessel density and decays at a constant rate δ_1, and that $Ang1$ is produced by the tumour at a constant rate α and decays at a constant rate δ_2. Note that another growth factor, $Ang2$, is not modelled here as an additional dimension, rather it is assumed to exist in a constant amount. Hence, it is represented as one of the constant parameters wherever relevant in the functions f_1, f_2, and f_3. Let us also introduce time delays τ_1, τ_2, and τ_3 for tumour proliferation/death, immature vessel formation/regression and destabilisation,

respectively. We get the system:

$$\begin{cases} \dot{N} = f_1(E_{\tau_1})N, \\ \dot{P}_1 = f_2(E)N - \delta_1 P_1, \\ \dot{P}_2 = \alpha N - \delta_2 P_2, \\ \dot{V}_1 = f_3(P_{1\tau_2})V_1 - f_4(P_2)V_1 + f_5(P_{2\tau_3})V_2, \\ \dot{V}_2 = f_4(P_2)V_1 - f_5(P_{2\tau_3})V_2, \end{cases} \tag{7.12}$$

where f_1, f_2, and f_3 satisfy (7.2), (7.4), and (7.5), respectively and

- f_4 is the maturation rate, it is a positive increasing function of P_2.
- f_5 is the destabilisation rate, it is a positive decreasing function of P_2 and satisfies
$$\lim_{P_2 \to \infty} f_5(P_2) = 0. \tag{7.13}$$

After making the substitutions $V_i \to E_i = V_i/N$ and $E_2 \to E = E_1 + E_2$ we get the system

$$\begin{cases} \dot{N} = f_1(E_{\tau_1})N, \\ \dot{P}_1 = f_2(E)N - \delta_1 P_1, \\ \dot{P}_2 = \alpha N - \delta_2 P_2, \\ \dot{E}_1 = f_3(P_{1\tau_2})E_1 - f_4(P_2)E_1 + f_5(P_{2\tau_3})(E - E_1) - f_1(E_{\tau_1})E_1, \\ \dot{E} = f_3(P_{1\tau_2})E_1 - f_1(E_{\tau_1})E. \end{cases} \tag{7.14}$$

For each set of parameters which determine f_1, f_2, f_3, f_4, and f_5, the model has one fixed point $Q^{(2)} = (N^{(2)}, P_1^{(2)}, P_2^{(2)}, E_1^{(2)}, E^{(2)})$ with $N^{(2)} > 0$ given by the conditions

$$\begin{aligned} & f_1(E^{(2)}) = 0\,, \qquad f_3(P_1^{(2)}) = 0\,, \qquad N^{(2)} = \frac{\delta_1 P_1^{(2)}}{f_2(E^{(2)})}, \\ & P_2^{(2)} = \frac{\alpha \delta_1 P_1^{(2)}}{\delta_2 f_2(E^{(2)})}\,, \qquad E_1^{(2)} = \frac{f_5(P_2^{(2)})E^{(2)}}{f_4(P_2^{(2)}) + f_5(P_2^{(2)})} \end{aligned} \tag{7.15}$$

while exercising on the system the same analysis (full analysis appears in [48]), we find that for every pair $(\tau_1, \tau_2) \neq (0, 0)$, there always exist parameter sets such that $Q^{(2)}$ is a Hopf bifurcation point of the system (7.14).

We summarise the results about $3 - D$ and $5 - D$ models in the following proposition:

Proposition 7.3.1 *The ODE systems (7.10) and (7.14) admit a Hopf bifurcation point if and only if at least one of the time delays is nonzero.*

7.3.1.5 Further extension of the model

We further extended the model, by allowing $Ang2$ not to be constant, but rather to be produced by immature vessels, thus being a function of their quantity. Hence, we introduced an additional dimension to the model. In this case, the maturation/destabilisation process depends both on $Ang1$ and on $Ang2$. Here too, time delays were implemented. The analysis of this last system (not shown), demonstrated again the existence of Hopf points when at least one of the time delays is nonzero.

Another possibility for extension that was exercised, was the addition of protein consumption by growing vessels, rather than assuming it is merely constantly cleared by entities outside the modelled system. This was performed on the $3-D$ model without time delay and had no Hopf points, similarly to other systems with no time delay.

7.3.1.6 Interpreting the results

A biological observed phenomenon is a given, for which we seek an explanation or at least a description. In the case of the empirical results presented above, a major apparent phenomenon is an oscillatory behaviour. One of the means for analytically describing oscillatory behaviour is a system of equations with Hopf bifurcation points. Introduced above were several modelling suggestions describing angiogenesis, with or without time delays. As demonstrated, whenever time delay was introduced into the system, Hopf points were found, leading to oscillatory behaviour. This might mean that the more appropriate candidate for describing the biological system in question is the alternative that includes time delays. While it is recognised that time delay will often elicit Hopf points, here it was shown that the latter were to be found for any angiogenesis model with time delay. Note that the introduction of time delay was also mandatory for the analysis of the empirical results. These conclusions underline the possible significance of time delays in tumour dynamics.

7.3.2 A Discrete Model

7.3.2.1 Description of the algorithm

The algorithm of the discrete mathematical model includes six major processes simultaneously, namely tumour cell proliferation and death, immature vessel formation and regression, immature vessel maturation, and mature vessel destabilisation (the complete algorithm is described in detail in [50,51]). A simplified scheme of the algorithm (Figure 7.5) presents three interconnected modules, within which these six subprocesses are included: tumour growth (proliferation and death), angiogenesis (immature vessel growth and regression), and maturation (formation and destabilisation of mature vessels). Each of these modules operates on three scales: molecular,

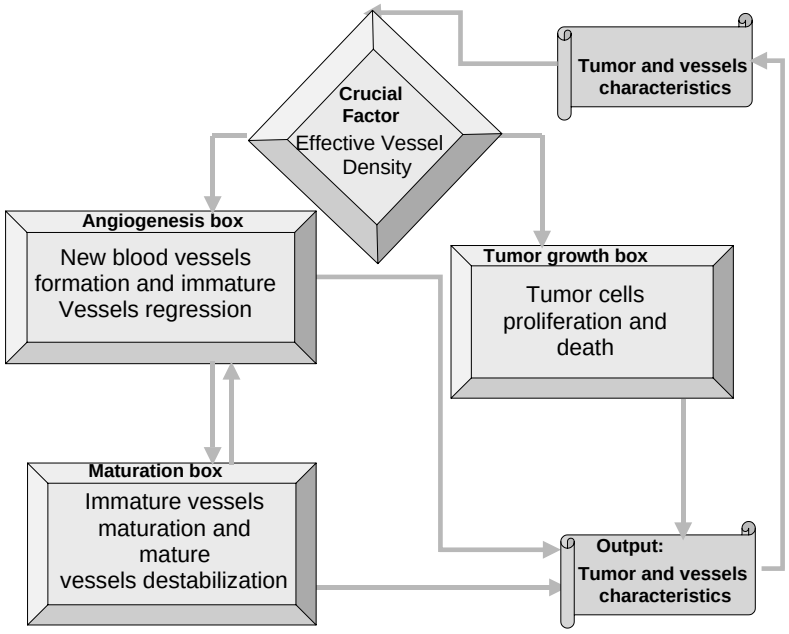

Figure 7.5

The simplified algorithm describing the principal interactions affecting a vascular tumour growth. It defines three major entities indicated as "boxes;" tumour growth, immature vessels (angiogenesis), and mature vessels, and conveys the interrelationships between them. These interactions occur across three organisation scales: molecular, cellular, and organ level (for a full description of this algorithm, we refer to [50,51]).

cellular and macroscopic (tissue level).

The tumour module consists of tumour cell proliferation and death, further subdividing into:

- a genetically determined block, which is cell type-specific and does not vary in time, and
- a block which is time-variant and nutrient-dependent.

A crucial factor in the tumour module is the density of the total perfused vasculature (to be denoted effective vascular density, EVD). Proliferation rate is directly proportional to EVD and death rate is inversely proportional to it. In addition, proliferation and death rates are both nutrient-dependent [52]. Two additional quantities are calculated in this module, namely VEGF and PDGF production. They are both

inversely related to EVD so that aggravation of nutrient depletion results in increasing secretion of proangiogenic factors [7–9]. The tumour growth module interacts with the angiogenesis and the maturation modules via the relevant regulatory proteins.

In the angiogenesis module we calculate immature vessel volume. Immature vessel volume increases proportionally to VEGF concentration, once above a given threshold level, and regresses if VEGF is below a given, possibly different, threshold level. The latter threshold is generally referred to as "survival level" [30] to [33].

In the maturation module, we calculate mature vessels volume according to pericyte concentration [52,53] and according to Ang1/Ang2 ratio [54]. Pericytes proliferate proportionally to PDGF concentration [34,35]. Ang1 and Ang2 are continuously secreted by tumour cells and immature vessels, respectively [36,37,41,42,52, 53,55]. Additionally, Ang2 can be secreted by tumour cells, if the latter are nutrient-depleted [37]. We assume that maturation of immature vessels occurs if pericytes concentration and Ang1/Ang2 ratio are above their respective threshold levels, otherwise, if under these thresholds, immature vessels do not undergo maturation, while mature vessels undergo destabilisation and become immature [38] to [42].

7.3.2.2 Numerical calculations

The above algorithm is precisely described mathematically by a large set of formulas underlying each and every interaction in Figure 7.5 and more. This full mathematical model has been studied by numerical simulations only, as it is much too complex to be tractable to mathematical analysis (but see the analysis of less complex forms of the model in the previous section, "continuous models"). Some simulation results of the full model are presented in section 7.4.1.

Recursive numerical simulations of the model have been performed. Note that at this point, we needed to define the parameter space within which simulations will be conducted. Owing to the relative novelty of the field of angiogenesis, and hence, the scarcity of experimentally evaluated parameters, we used arbitrary dimensionless units for all model parameters. Initial conditions were 100 tumour units and zero vascular densities. Calculation step duration is equivalent to generation time of tumour cells, that is, to one cell cycle.

At every time step the model calculates the tumour size, which is determined as a function of tumour cell number, the number of free endothelial cells and pericytes, the concentrations of the regulatory factors (VEGF, PDGF, Ang1, and Ang2), and the volume of immature and of mature vessels.

In addition, immature and mature vessel densities (the volumes of corresponding vessels divided by tumour size) are calculated and summed into EVD. EVD is defined as the sum of the densities of any perfused vessels, whether immature or mature. For simplicity we assume here that perfusion efficiency is the same in immature and mature vessels. However, this constraint can be easily alleviated.

The model assumes several threshold-dependent and ratio-dependent effects of regulatory factors, as follows:

- A threshold of VEGF concentration above which endothelial cell proliferation takes place
- A threshold of VEGF concentration under which endothelial cells, either incorporated into immature blood vessels or unattached, undergo apoptosis
- A threshold concentration of free unattached pericytes above which immature vessels can mature
- Ang1/Ang2 ratio above which immature vessels mature and below which mature vessels are destabilised

7.4 Applying the Models: From Theory to the Clinic

One can utilise angiogenesis mathematical modelling to serve several purposes. As we saw above, empirical data may reflect very intriguing phenomena, the analysis of which is enabled using such tools. The better understanding of such phenomena will lead to novel ideas for research and therapy. In addition, this work gives new options for the evaluation of novel antiangiogenic therapies. This will be demonstrated in the results section below. Clearly, if one wishes to apply such models for pharmaceutical or clinical uses, an additional module will have to be added to them, addressing the question of the pharmacodynamics and pharmacokinetics of the modelled drugs. This will be addressed towards the end of this section.

7.4.1 Simulation Results

The computer simulation of the tumour growth and angiogenesis discrete model described above, was represented as time series of the measured quantities: the effective vascular density, the tumour size, the concentrations of VEGF, Ang1 and Ang2, Ang1/Ang2 ratio, the immature and mature vessel volume, and more. Time is measured in cell cycles, while values on the y-axes in all graphs are expressed in arbitrary units.

7.4.1.1 Simulation of antiangiogenic and antimaturation therapies

One interesting application of this model may be the simulation of "prototypical" antiangiogenic and antimaturation therapies. Continuous administration was simulated, of two different hypothetical drugs affecting vascular dynamics, namely a VEGF-production inhibitor (drug A) and an Ang1 production inhibitor (drug B).

Monotherapy by drug A only, drug B only, or combination of both drugs, were simulated and compared with disease progression with no intervention. The different therapies were applied under similar conditions in terms of initial tumour size, reaction coefficients, and initial total vessel volume. For each of the initial sets, the simulated aspects of tumour growth were vascular volume, concentrations of Ang1 and Ang2, and tumour size. Those are presented in Figures 7.6 and 7.7 as a function of time in the upper, middle, and lower graphs, respectively.

However, for some of these therapies, three different sets of initial proportions of immature vessels were applied, being 50%, 95%, or 5%, as will be indicated in each of the examples herein.

Figure 7.6 shows simulation results of tumor growth characteristics under no therapy (left), drug A monotherapy (middle), and drug B monotherapy (right). The therapies were applied under the same initial conditions for the disease and under the assumption that initial volumes of immature and mature vessels were equal. One may notice in these simulations that drug A therapy (middle) slows down tumour growth without eliminating it. Rather, tumour size continues to increase nonlinearly, even under a prolonged treatment period and increased drug dose (not shown). As for drug B, (right) its application seems to cause a substantial deceleration in tumour growth, yet when observed under a smaller scale (inserts of Figure 7.6, right), one may appreciate that the trend of nonlinear growth still exists.

Figure 7.7 presents the simulation results of the combination therapy of drugs A and B with 50%, 95%, and 5% initial immature vessel percentage (left, middle, and right, respectively). All combination treatments simulated appear to cause prolonged suppression of tumour growth and a significant linear decrease in average tumour size. In the case of the immature vessel density being 95% (Figure 7.7, middle), the suppression was much more remarkable. Hence, in addition to having an advantage over the monotherapies simulated (Figure 7.6), it is demonstrated that the relative deceleration in tumour growth caused by this particular combination therapy is a function of the initial relative proportion of immature/mature vessel volume. Thus, the suggested combination therapy seems to yield an even better result when the proportion of immature vessels is relatively large (Figure 7.7, middle). Note that this general result is independent of initial conditions, other than immature vessel proportion.

In order to check whether the phenomenon of oscillatory growth behaviour, is also apparent in simulation results, two simulations were performed, the results of which are brought in Figure 7.8. The difference in the setting of the system between the two simulations, is in the intrinsic level of Ang1 which is defined as genetically determined. This Ang1 level was assumed to be 1 unit (upper Figure 7.8) or 35 units (lower Figure 7.8). All other simulation conditions (parameters) were set as equal in both cases. On the right side of Figure 7.8, simulated tumour growth is presented (size as a function of time in days). Observing the left part of Figure 7.8, one may appreciate that this simulated tumour growth is characterized by fluctuations, in both upper and lower parts (Ang1 equals 1 and 35 respectively). This is coherent with the findings presented in section “defining the challenge” where such fluctuations were demonstrated in the experimental results.

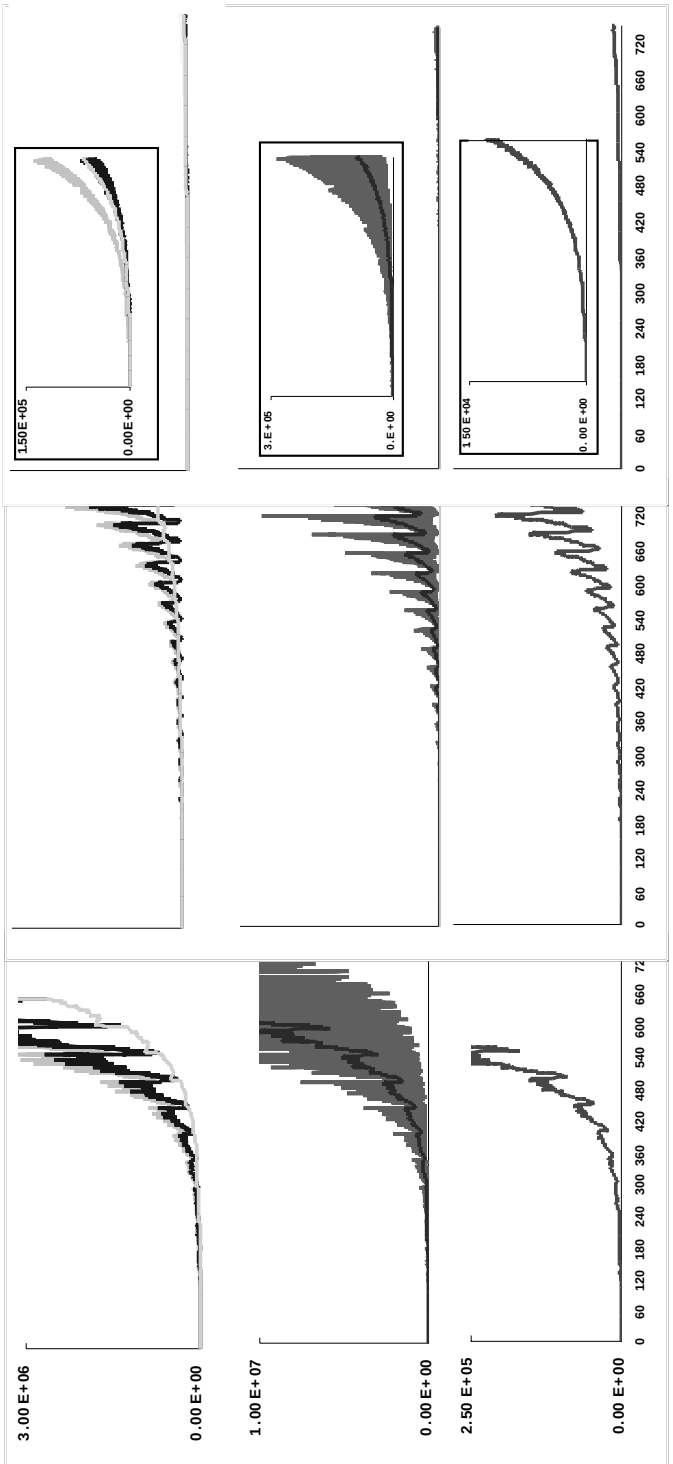

Figure 7.6
Simulation results of tumour growth under no therapy (left), drug A monotherapy (middle) and drug B monotherapy (right), where initial immature and mature vessel volume are assumed to be equal. Vascular volume, concentrations of Ang1 and Ang2 and tumour size are displayed in upper, middle and lower graphs, respectively. Inserted in the right column graphs are smaller scale magnifications of the larger scale results.

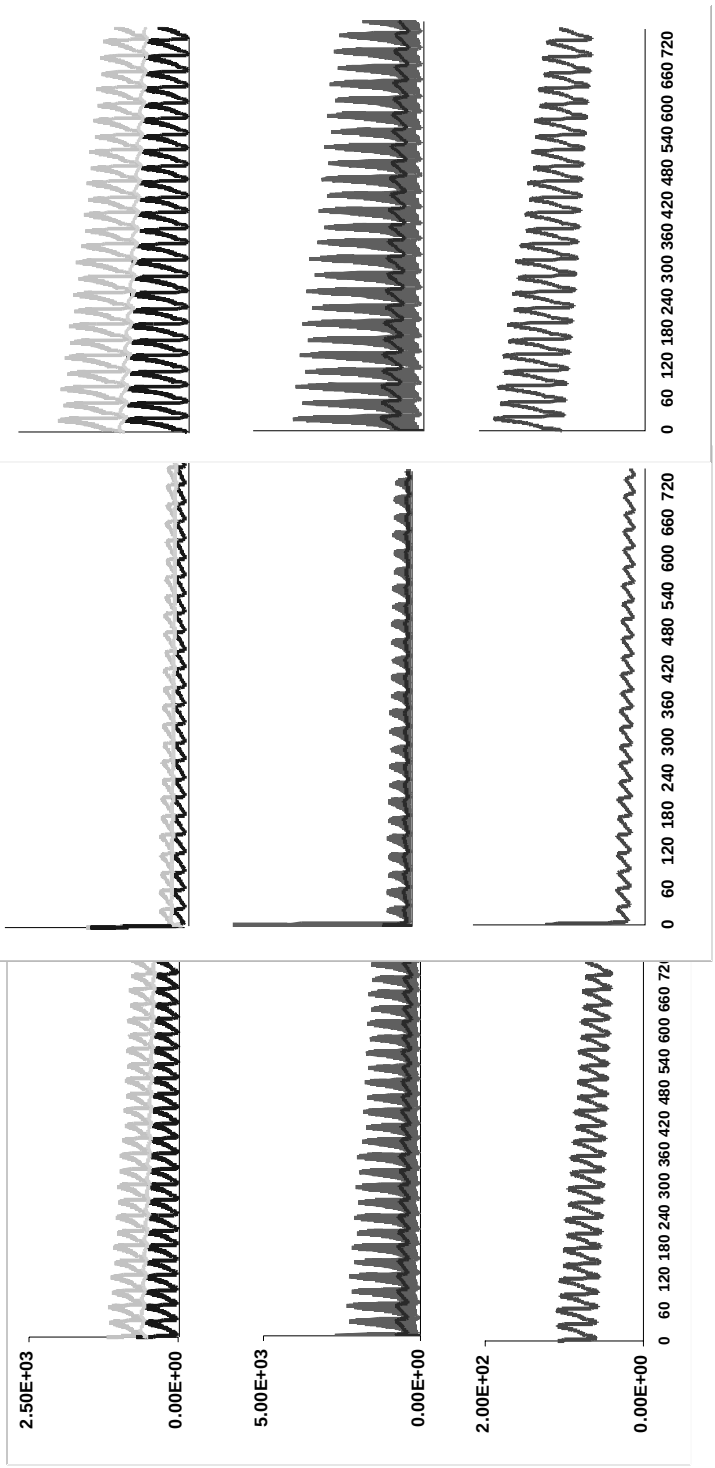

Figure 7.7
Simulation results of tumour growth under combination therapy of drug A and drug B. Initial conditions were equal except for immature vessel percentage, being 50%, 95% and 5% (left, middle, and right, respectively). Vascular volume, concentrations of Ang1 and Ang2 and tumour size are presented in upper, middle, and lower graphs, respectively.

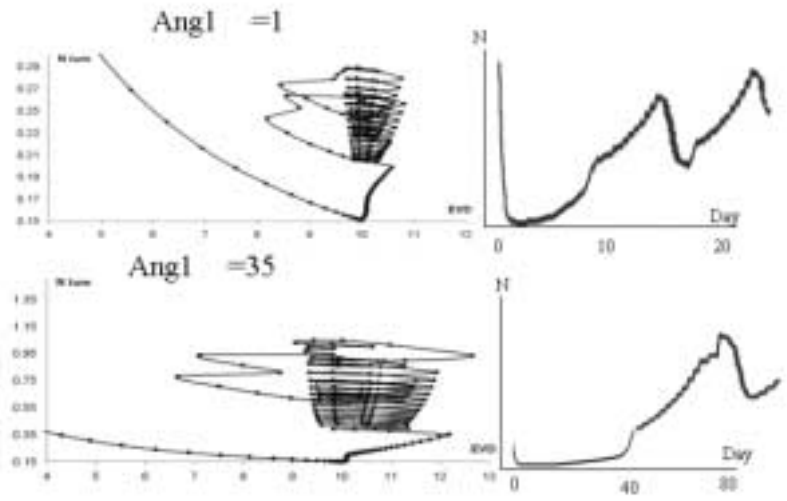

Figure 7.8

Results of two simulated situations, where the difference in the setting of the system is in the intrinsic level of Ang1. It was assumed to be 1 unit (upper) or 35 units (lower). Left: Phase plane representation of simulation results, showing EVD (x axis) as a function of tumour size ($Ntum$, y axis). (See phase plane representation of the experimental results in Figure 7.4). Right: Simulation results of tumour growth as a function of time in days.

In the first example above one may see how the utilization of the discrete mathematical model may help exploring therapy options and coming across new ideas to be further empirically tested. In the latter example, we have demonstrated the appearance of oscillatory growth phenomena in simulations of the discrete model. Similar phenomena were observed in the preceding section "analysis of experimental results."

7.4.2 Devising Drug Pharmacokinetic and Pharmacodynamic Models for Angiogenesis Simulations

One of the purposes in modeling angiogenesis is to predict the outcomes of a treatment, using a known drug and a well defined schedule. Once this is achieved, the model could be used for more sophisticated tasks, e.g., exploring new drugs or novel treatment protocol options for existing drugs.

7.4.2.1 The general structure

In order to make all these applications possible, we have to implement drug pharmacokinetics (PK) and pharmacodynamics (PD) as a part of the selected angiogenesis model. The PK model enables calculating drug concentration in the tissues where the drug effect occurs or in any other modeled compartments. The drug PD model accounts for the interaction between the drug and the modeled disease. The PD model interacts with the drug PK model, correlating the drug effect on the system to its concentration.

The drug PK can be modeled by one of the classical PK models [56], chosen according to the properties of the drug. The drug PK model includes a description of drug delivery and absorption, drug distribution in the body (both in the central compartment and in the peripheral compartments) and drug elimination from the body. The design of the PK model is adapted to the specific properties of the modeled drug. Thus, delivery method, absorption characteristics, number and nature of distribution compartments, the exchange between the compartments, and the metabolism and elimination patterns are chosen according to the information we have on the drug.

The drug PD model applies the drug effects to all the components of the mathematical models which simulate the biological processes of the target tissues. The effect of the drug is a function of the drug concentration in the target tissue or in the central compartment. In terms of the model, this effect can be expressed as a change in values of certain variables (e.g., the inhibition of production of a substance can be represented as a reduction of its production rate). Practically any drug effect can be described within this framework, given that the affected cell population or substance is represented in the disease model. Consequently, the same model can serve for describing the side-effects of the drug, which might require implementation of additional compartments simulating the tissues where the side effects take place.

7.4.2.2 Implementing PK/PD in the cancer model

Below we describe an example of drug PK and PD implementation in our angiogenesis model. The drug administration device in this example is a tablet. The drug is absorbed from the device by a first-order kinetics process, and enters the central compartment, which represents the blood. The volume of distribution of the drug (Vd) is not constant. Rather, it is elevating as a function of the drug amount. This represents the effect of a concentration-dependent drug binding by tissue proteins. In addition to the central compartment (blood), the model includes two peripheral compartments. One of the two represents the target tissue (in our case the tumour), where the drug concentration defines the effect of the drug on the disease. The drug concentration in the target tissue can differ from that in the blood. The rate of exchange between the blood (central compartment) and the tumour (target peripheral compartment), and so the resulting target tissue drug concentration, depends on the tumour tissue perfusion. The second peripheral compartment represents an additional distribution compartment for the drug. While differing from the central compartment in its drug distribution properties, it is implemented in order to complete the simulation of the drug pharmacokinetics and plays no role in the effect of the drug on the dis-

ease (pharmacodynamics). The clearance of the drug from the body is described by elimination from the central compartment by a first order kinetics process.

The drug effect is a function of the drug concentration in the target compartment. This function is of a sigmoid type: an increase in drug concentration leads to an increase in the effect, with saturation. In our example, the drug has three independent effects: (i) reducing the proliferation rate of the tumour cells, (ii) increasing the apoptotic rate of the tumour cells, and (iii) inhibiting VEGF production by the tumour cells. All these effects are expressed as sigmoid-like concentration-dependant functions, altogether yielding the resulting effect of the treatment.

7.5 Discussion

The complexity of angiogenesis and its significance in potential cancer therapy are well recognised. In experimental data brought here, several growth behaviours have been observed. Rapid tumour growth seems to have coincided with large ranges of vessel densities. In addition, growth seemed to be either in progress or in regress with no apparent direct relation with vessel density at the time of measurements. We have identified an oscillatory behaviour of tumour size in the periods in which growth rate was mild. This oscillatory behaviour may represent a limit-cycle fixed point, where both tumour size and vessel density fluctuate with a relatively fixed amplitude. Since there is a mutual effect of these two processes, it would be difficult to pinpoint cause and effect relationships. Still, one should expect to find some cyclic behaviour in the interaction of these two processes. The graphics of the relation between vessel density measurements and tumour size measurements, as it unfolds with time, are presented in Figure 7.4. In Figure 7.4 (lower), where an assumption of time delay was implemented, an oscillatory behaviour was observed, suggesting an interdependent path of development for these two processes. The concept of time delay falls into place with the biological intuition that there is a time gap between the appearance of the stimulus and the response to it. It also falls to reason that the duration of such a time gap would be variable between individuals, a function of genetic or environmental variability.

In addition, the fact that contrasting growth trends were observed under the same vessel density indicates that tumour growth is not a simple function of vessel density. Rather, growth rate is a function of several coexisting effects. This stresses the significance of separating the analysis of the involved processes, such as the dynamics of mature vs. immature vessels, or functional vessels, and checking the role of each one of them in controlling tumour growth status. Also, it is very likely that different time delays should be considered when checking the correlation with the tumour growth of each of the separate processes (e.g., the influence on growth of immature vs. mature vessels, may be kinetically different). The comparison of

time delays between individual cases and between different effectors, is a substantial issue to be addressed in future work.

Tumour growth and angiogenesis were modelled both in an analytical continuous way and in a discrete way, later implemented into a computer simulation.

As discussed already, the analytical model can aid in understanding the phenomena under research, but carries with it an inherent limit on complexity. Analysing the continuous models, we have shown that only if time delay is implemented into the models, is it possible to identify Hopf points. Hopf points are stable fixed points, which potentially can account for situations in which tumour size does not progress, rather it fluctuates between maxima and minima that are relatively similar. The latter result underlies the global properties of angiogenic dynamics, and supports the significance of time delay in the description of this process. It is also important for showing how connected the mathematical description brought herein is to the biological reality.

The discrete modelling proves to be an apparatus enabling the interactive integration of many different processes which occur on different biological organisation levels. We showed here that such an apparatus is essential for incorporating the high level of complexity in the description of the relevant processes. Hence, this provides an opportunity to study empirical phenomena, novel antiangiogenic drugs, new drug combinations, new drug schedules, etc. Some of the results are summarised herein (see [51] for complete results) and suggest that the combination of antiVEGF and antiAng1 therapies may be advantageous over the possibility of adopting a regime applying just one of them.

Looking into future work, we suggest that mathematical modelling can be highly instrumental in unravelling the complexity of cancer growth and therapy. Modelling tools may be used both for reaching a better understanding of the causality of the processes in question, and for easily testing new drugs. Our discrete mathematical algorithm suggests that there are many points in this complex dynamics, where suppression or stimulation by new drugs can be examined. This would require the addition of pharmacokinetics and pharmacodynamics modelling to the work already presented here.

7.6 Conclusions

Angiogenesis dynamics is highly complex, including several processes which operate on different levels of the biological system. Fragile new vessels form and regress, and at the same time can be covered by pericytes and mature into more resilient forms which, subsequently, may still be destabilised. The rates of these dynamics are determined by a plurality of factors, such as the genetic characteristics of the organism, the availability of nutrients at certain moments, and of proteins like VEGF and other stimulatory factors, affecting endothelial cell proliferation and

migration during other moments. Moreover, the different dynamical processes are interconnected by several feed-back loops, which can accelerate some of them while decelerating others. In order to concurrently account for the interactive dynamics of the relevant nutrients and growth factors, the different cell types, tumour mass, and the various blood vessel types, the model of angiogenesis should necessarily be a multi-scale one. Several continuous models with increasing complexity were discussed here. They were all shown to require the inclusion of time delays in order to identify Hopf points, which possibly represent the oscillatory phenomena observed empirically. The discrete model discussed here, included a highly complex description of the relevant processes. This description served as a basis for constructing a simulation apparatus which offers further research opportunities. One such application was presented here, suggesting a major advantage to the combination of antiVEGF and antiAng1 therapy over a monotherapy, which uses just one of such drugs. It is our hope that cancer therapy will be aided by using modelling tools such as those presented here, both for reaching a better understanding of the processes in question and for easily testing new therapies.

Acknowledgments

We are much obliged to Prof. Michal Neeman for providing the experimental data analysed in this work and for a very useful discussion. We are also indebted to Assaf Gilead for aiding in data analysis. The work was supported by the Chai Foundation, and the European Union Commission through the Human Potential Programme, Contract No HPRN-CT-2000-00105. Dr. Arakelyan is a recipient of the Shapira Scholarship from the Center of Absorption in Science of the Israeli Ministry of Absorption.

7.7 References

[1] Folkman, J., Angiogenesis in cancer, vascular, rheumatoid, and other disease, *Nat. Med.* 1, 27, 1995.

[2] Folkman, J., Tumour angiogenesis: therapeutic implications, *N. Engl. J. Med.* 285, 1182, 1971.

[3] O'Reilly, M.S. et al., Angiostatin: a novel angiogenesis inhibitor that mediates the suppression of metastases by a Lewis lung carcinoma, *Cell* 79, 315, 1994.

[4] O'Reilly, M.S. et al., Endostatin: an endogenous inhibitor of angiogenesis and tumour growth, *Cell* 88, 277, 1997.

[5] Carmeliet, P. and Jain, R.K., Angiogenesis in cancer and other diseases, *Nature* 407, 249, 2000.

[6] Yangopoulos, G.D. et al., Vascular-specific growth factors and blood vessel formation, *Nature* 407, 242, 2000.

[7] Kerbel, R.S., Tumour angiogenesis: past, present, and the near future, *Carcinogenesis* 21, 505, 2000.

[8] Danielsen, T. and Rofstad, E.K., The constitutive level of vascular endothelial growth factor (VEGF) is more important than hypoxia-induced VEGF upregulation in the angiogenesis of human melanoma xenografts, *Brit. J. Cancer* 82(9), 1528, 2000.

[9] Dor, Y., Porat, R., and Keshet, E., Vascular endothelial growth factor and vascular adjustments to perturbations in oxygen homeostasis, *AJP-Cell Physiology* 280, 1367, 2001.

[10] Ikeda, E. et al., Hypoxia-induced transcriptional activation and increased mRNA stability of vascular endothelial growth factor in C6 glioma cells, *J. Biol. Chem.* 270, 19761, 1995.

[11] Lin, P. et al., Anti-angiogenic gene therapy targeting the endothelium-specific receptor tyrosine kinase Tie-2, *Proc. Natl. Acad. Sci.* 95, 8829, 1998.

[12] Diaz Flores, L. et al., Microvascular pericytes: a review of their morphological and functional characteristics, *Histol. Histopathol.* 6, 269, 1991.

[13] Breier, G. et al., Expression of vascular endothelial growth factor during embryonic angiogenesis and endothelial cell differentiation, *Development* 114, 521, 1992.

[14] Shweiki, D. et al., Vascular endothelial growth factor induced by hypoxia may mediate hypoxia-initiated angiogenesis, *Nature* 359, 843, 1992.

[15] Ferrara, N. and Henzel, W.J., Pituitary follicular cells secrete a novel heparin-binding growth factor specific for vascular endothelial cells, *Biochem. Biophys. Res. Commun.* 161, 851, 1989.

[16] Ferrara, N. et al., Molecular and biological properties of the vascular endothelial growth factor family of proteins, *Endocr. Rev.* 13, 18, 1992.

[17] Ferrara, N. et al., Heterozygous embryonic lethality induced by targeted inactivation of the VEGF gene, *Nature* 380, 439, 1996.

[18] Carmeliet, P. et al., Abnormal blood vessel development and lethality in embryos lacking a single VEGF allele, *Nature* 380, 435, 1996.

[19] Barleon, B. et al., Migration of human monocytes in response to vascular endothelial growth factor (VEGF) is mediated via the VEGF receptor flt-1, *Blood* 87, 3336, 1996.

[20] Neufeld, G. et al., Vascular endothelial growth factor (VEGF) and its receptors, *FASEB* 13, 9, 1999.

[21] Jain, R.K., Normalizing tumour vasculature with anti-angiogenic therapy: a new paradigm for combination therapy, *Nat. Med.* 7, 987, 2001.

[22] Agur, Z., Abiri, D., and Van der Ploeg, L.H.T., Ordered appearance of antigenic variants of African trypanosomes, explained in a mathematical model based on a stochastic process and immune-selection against putative switch intermediates, *Proc. Natl. Acad. Sci. USA* 86, 9626, 1989.

[23] Agur, Z. et al., Pulse mass measles vaccination across age cohorts, *Proc. Nat. Acad. Sci. USA* 90, 11698, 1993.

[24] Shulgin, B., Stone, L., and Agur, Z., Pulse vaccination strategy in the SIR endemic model, *Bull. Math. Biol.* 60, 1123, 1998.

[25] Agur, Z., Clinical trials of Zidovudine in HIV infection, *Lancet* 2, 734, 1989.

[26] Agur, Z. et al., Zidovudine toxicity to murine bone marrow may be affected by the exact frequency of drug administration, *Exp. Hematol.* 19, 364, 1991.

[27] Agur, Z., Arnon, R., and Schechter, B., Effect of the dosing interval on survival and myelotoxicity in mice treated by Cytosine arabinoside, *Eur. J. Cancer* 28A, 1085, 1992.

[28] Ubezio, P. et al., Increasing 1-b-D-arabinofuranosylcytosine efficacy by scheduled dosing intervals based on direct measurement of bone marrow cell kinetics, *Cancer Res.* 54, 6446, 1994.

[29] Agur, Z., Resonance and anti-resonance in the design of chemotherapeutic protocols, *J. Theor. Medicine* 1, 237, 1998.

[30] Benjamin, L.E. and Keshet, E., Conditional switching of vascular endothelial growth factor (VEGF) expression in tumours: induction of endothelial cell shedding and regression of hemangioblastoma-like vessels by VEGF withdrawal, *Proc. Natl. Acad. Sci.* 94, 8761, 1997.

[31] Jain, R.K. et al., Endothelial cell death, angiogenesis, and microvascular function after castration in an androgen-dependent tumour: role of vascular endothelial growth factor, *Proc. Natl. Acad. Sci.* 95, 10820, 1998.

[32] Holash, S.J., Wiegandand, G.D., and Yancopoulos, G.D., New model of tumour angiogenesis: dynamic balance between vessel regression and growth mediated by angiopoietins and VEGF, *Oncogene* 18, 5356, 1999.

[33] Gilead, A. and Neeman, M., Dynamic remodeling of the vascular bed precedes tumour growth: MLS ovarian carcinoma spheroids implanted in nude mice, *Neoplasia* 1, 226, 1999.

[34] Benjamin, L.E. et al., Selective ablation of immature blood vessels in established human tumours follows vascular endothelial growth factor withdrawal, *J. Clin. Invest.* 103, 159, 1999.

[35] Benjamin, L.E. et al., A plasticity window for blood vessel remodeling is defined by pericyte coverage of the preformed endothelial network and is regulated by PDGF-B and VEGF, *Development* 125, 1591, 1998.

[36] Currie, M.J. et al., Angiopoietin-1 is inversely related to thymidine phosphorylase expression in human breast cancer, indicating a role in vascular remodeling, *Clin. Cancer Res.* 7, 918, 2001.

[37] Koga, K. et al., Expression of angiopoietin-2 in human glioma cells and its role for angiogenesis, *Cancer Res.* 61, 6248, 2001.

[38] Davis, S. et al., Isolation of angiopoietin-1, a ligand for the Tie2 receptor, by secretion-trap expression cloning, *Cell* 87, 1161, 1996.

[39] Suri, C. et al., Requisite role of angiopoietin-1, a ligand for the TIE2 receptor, during embryonic angiogenesis, *Cell* 87, 1171, 1996.

[40] Maisonpierre, P.C. et al., Angiopoietin-2, a natural antagonist for Tie2 that disrupts *in vivo* angiogenesis, *Science* 277, 55, 1997.

[41] Audero, E. et al., Expression of angiopoietin-1 in human glioblastoma regulates tumour-induced angiogenesis, *Arterioscl. Thromb. Vasc. Biol.* 21, 536, 2001.

[42] Stratmann, A., Cell type-specific expression of angiopoietin-1 and angiopoietin-2 suggests a role in glioblastoma angiogenesis, *Am. J. Pathol.* 153, 1459, 1998.

[43] Abramovitch, R. et al., *In vivo* prediction of vascular susceptibility to vascular endothelial growth factor withdrawal: magnetic resonance imaging of C rat glioma in nude mice, *Cancer Res.* 59, 5012, 1999.

[44] Merbl, Y. et al., Analysis of murine experimental data describing tumour development, angiogenesis, and microvessel maturation, *in preparation.*

[45] Hahnfeldt, P. et al., Tumour development under angiogenic signaling: a dynamic theory of tumour growth, treatment response, and postvascular dormancy, *Cancer Res.* 59, 4770, 1999.

[46] Bellomo, N. and Preziosi, L., Modeling and mathematical problems related to tumour evolution and its interaction with the immune system, *Math. Comp. Modeling* 32, 413, 2000.

[47] De Angelis, E. and Preziosi, L., Advection-diffusion models for solid tumour evolution *in vivo* and related free boundary problem, *Math. Models Methods Appl. Sci.* 10, 379, 2000.

[48] Daugulis, P. et al., Hopf bifurcation analysis for angiogenesis models, *Discrete and Continuous Dynamical Systems* in press.

[49] Chicone, C., *Ordinary Differential Equations with Applications*, Springer-Verlag, Heidelberg, 1998.

[50] Arakelyan, L., Vainstain, V., and Agur, Z., Optimizing anti-angiogenic therapy using mathematical tools. *Proceedings of the American Society of Clinical Oncology (ASCO)* 21, 440a, 2002.

[51] Arakelyan, L., Vainstain, V., and Agur, Z., A computer algorithm describing the process of vessel formation and maturation, and its use for predicting the effects of anti-angiogenic and anti-maturation therapy on vascular tumour growth, *Angiogenesis*, in press.

[52] Darland, D.C. and D'Amore, P.A., Blood vessel maturation: vascular development comes of age, *J. Clin. Invest.* 103, 157, 1999.

[53] Ahmad, S.A. et al., Differential expression of angiopoietin-1 and angiopoietin-2 in colon carcinoma, *Cancer* 92, 1138, 2001.

[54] Goede, V. et al., Analysis of blood vessel maturation processes during cyclic ovarian angiogenesis, *Lab. Invest.* 78, 1385, 1998.

[55] Kakolyris, S. et al., Relationship of vascular maturation in breast cancer blood vessels to vascular density and metastasis, assessed by expression of a novel basement membrane component LH39, *Brit. J. Cancer* 82, 844, 2000.

[56] Gabrielsson, J. and Weiner, D., *Pharmacokinetics and Pharmacodynamics Data Analysis: Concepts and Applications*, 3rd Edition, Swedish Pharmaceutical Press, Stockholm, 2000.